Preliminary Study of a Low Noise Rotor

Natsuki KONDO, Hiroki NISHIMURA, Hideaki NAKAMURA,
Makoto AOKI, Tomoka TSUJIUCHI, Eiichi YAMAKAWA

Advanced Technology Institute of Commuter-helicopter, Ltd.
2 Kawasaki-cho, Kagamigahara, Gifu 504, Japan

Takashi AOYAMA, Shigeru SAITO

National Aerospace Laboratory
7-44-1, Jindaijihigashi-machi, Chofu, Tokyo 182, Japan

Abstract

This paper describes the design procedure of the low noise rotor developed by Advanced Technology Institute of Commuter-helicopter (ATIC) and presents the calculated aerodynamic and aeroacoustic characteristics of the rotor. The reduction of rotor rotational speed and the use of a 5-bladed rotor are the main concept for the design of the low noise rotor. However, the reduction of rotor rotational speed widens the stall region in the retreating side of a rotor and induces vibration. Therefore, a blade, which effectively delays the occurrence of stall, is newly developed by improving the characteristics of airfoil and tip planform. Two airfoils, AK080A and AK100D, and a tip planform, $J2_{mod}$, are designed and integrated into a blade, AT1. The aerodynamic and aeroacoustic analyses of the AT1 model rotor are performed using the several analytical methods which have been jointly developed by National Aerospace Laboratory (NAL) and ATIC. These analyses are performed in advance of the wind tunnel test that will be conducted at the German Dutch Windtunnel (DNW) in the beginning of 1998 using the 1/3-scaled model of the rotor. The results show that the new blade improves the rotor performance and reduces the rotor noise. The computed results in this study will be compared with the experimental data that will be obtained by DNW test.

Nomenclature

AR	: aspect ratio, R/c
C_l, C_L	: 2-D and 3-D lift coefficients
C_{lmax}	: 2-D maximum lift coefficient
C_d, C_D	: 2-D and 3-D drag coefficients
C_m, C_M	: 2-D and 3-D pitching moment coefficients
C_T	: rotor thrust coefficient
C_Q	: rotor torque coefficient
c	: chord length, m
M	: freestream Mach number
M_{dd}	: drag divergence Mach number
M_{tip}	: hover tip Mach number
R	: rotor radius, m
r	: radial station, m
t/c	: thickness ratio
V	: forward speed, kt
α	: angle of attack, deg.
α_{tpp}	: tip path plane tilt angle, deg.
θ_C	: collective pitch angle, deg.
θ_{1C}	: lateral cyclic pitch angle, deg.
θ_{1S}	: longitudinal cyclic pitch angle, deg.
θ_{TR}	: collective pitch angle of tail rotor, deg.
θ_t	: blade twist angle, deg.
μ	: rotor advance ratio
σ	: solidity
ϕ	: rotor azimuth angle, deg.

1. Introduction

Commuter helicopters are expected as a means of transportation from cities to cities, but they have not been effectively used yet. One of the reasons is the noise problem in residential areas. Present external noise standards for civil helicopters were defined by the International Civil Aviation Organization (ICAO) in 1985[1]. However, increasing helicopter market and increasing low altitude operation raise global concern about helicopter noise. The public pressure will make the noise limit more stringent in the near future. Therefore, the development of quiet civil helicopters is highly required and the noise reduction techniques play a more and more important part in the recent rotor design of commuter helicopters[2].

The external noise of a helicopter is mainly generated by main and tail rotors. In recent years, a ducted tail rotor or a no tail rotor system have been developed and utilized as an anti-torque system of helicopters. In Japan, a low noise ducted tail rotor has been applied to a light observation helicopter, XOH-1, developed by Technical Research and Development Institute (TRDI) and Kawasaki Heavy Industries, Ltd. It is reported that these techniques reduce the tail rotor noise effectively[3][4]. Therefore, we focus our major research efforts on the noise reduction of the main rotor.

In 1994, Advanced Technology Institute of Commuter-helicopter (ATIC) was established in Japan and

started the research activities for external noise and flight safety problems of helicopters. The final objective of the research by ATIC is to obtain a rotor technologies by which the external noise can be reduced at least 10 EPNdB less than the present ICAO noise limits. The noise reduction techniques are investigated experimentally and analytically. The research topics in ATIC are the followings:

a) Development of prediction techniques of rotor noise and performance,
b) Improvement of airfoil and tip planform,
c) Trade-off study between noise and performance,
d) Study of higher harmonic control (HHC),
e) Study of active flap control,
f) Development of variable rotational speed system,
g) Study of flight operation for noise reduction,
h) Development of flow visualization techniques (e.g. LDV and PIV).

The results of these researches have been integrated into a 1/3-scale model rotor. The aerodynamic and aeroacoustic characteristics of the rotor will be studied experimentally in the German Dutch Windtunnel (DNW). The model rotor test in DNW is separated into two phases. The first phase will be conducted in the beginning of 1998 and the second phase in 2000.

This paper describes the design procedure of the low noise rotor developed by ATIC and presents the calculated aerodynamic and aeroacoustic characteristics of the rotor. These calculations are performed using the several analytical methods which have been jointly developed by National Aerospace Laboratory (NAL) and ATIC. The research topics concerned in this paper are a) and b). The detailed information about the topics of d), e), and h), is mentioned in the references (5) and (6). The efforts on the research of topic c) will be made mainly after the first DNW test and the result will be applied to the design of the model rotor that will be tested in the second DNW test. The topics of f) and g) have been studied but the results have not been published yet.

2. Calculation Method

2.1 Rotor trim code

Trimmed condition and performance of a rotor or a rotorcraft are calculated using CAMRAD II based on the lifting line theory. CAMRAD II is a comprehensive analytical code for rotorcraft aerodynamics and dynamics developed by Johnson Aeronautics. In CAMRAD II, the sectional load and moment based on 2-D airfoil characteristics obtained by wind tunnel tests are used to calculate aerodynamic forces. The rotor wake is modeled by discrete vortex elements and the velocity induced by the rotor wake is computed by the Biot-Savart law. The blade structural motion is computed by the beam theory.

Figure 1 shows the predicted power of BK117 compared with flight test data[7]. It is indicated that CAMRAD II predicts the power required very well. Figure 2 shows the predicted control inputs compared with the flight test data[7]. The calculated results are in reasonable agreement with the measured ones except for θ_{1C} in high speed forward flight conditions. It is confirmed by some sensitivity studies that the discrepancy of θ_{1C} dose not strongly affect the results of noise and performance predictions.

2.2 CFD codes

The aerodynamic analysis in this study is performed using the Euler and Navier-Stokes codes[8][9] developed by NAL. The Navier-Stokes code is used only for the investigation in which the effect of blade tip shapes on tip-vortex structure in hover is analyzed.

The governing equations used in the codes are three dimensional Euler and Navier-Stokes equations in the blade fixed rotating Cartesian coordinate system. The numerical method to solve each of the governing equations is an implicit finite-difference scheme. A higher-order upwind scheme based on TVD is applied for the inviscid terms of the explicit right-hand side. The q-ω two-equation turbulence model is applied to calculate turbulent eddy viscosity. To obtain the unsteady solution in the forward flight condition of a helicopter rotor, the Newton iterative method is added. In the beginning of the calculation, the steady calculation is conducted at $\phi = 90^{\circ}$ using the implicit time-marching method. Then, the unsteady calculation is started from this initial condition. The periodic converged solutions for non-lifting and lifting blades are obtained at about $\phi = 200^{\circ}$ and 360°, respectively.

2.3 Aeroacoustic codes

2.3.1 Total external noise

A calculation method for total external noise of helicopters has been developed in order to predict the effective perceived noise level (EPNL) prescribed in ICAO Annex 16[1]. The noise sources considered for the total external noise prediction are rotational noise of main and tail rotors, and broadband noise of main rotor. The rotational noise is defined as the noise without broadband and impulsive noises in this study. The broadband noise of tail rotor and engine noise are ignored because their influence on the total external noise is very small.

The calculation of the rotational noise consists of following three steps: 1) trim analysis using CAMRAD II, 2) aerodynamic analysis using a potential code based on the Moriya's method[10], and 3) noise analysis using an aeroacoustic code[11] based on the Ffowcs Williams and Hawkings (FW-H) formulation without quadrupole term. The broadband noise of

main rotor is predicted using a semi-empirical method based on 2-D measurement data of NACA0012 airfoil. This method was originally proposed by Brooks, et al[12]. The sectional angle of attack which is the input data for the broadband noise prediction is obtained by CAMRAD II.

Figure 3 shows the calculated noise spectrum for BK117 compared with experimental data in a forward flight condition. The agreement between the calculated and the measured results is reasonable. The detail of the flight test is reported in reference (13).

ICAO requires three flight patterns, flyover, take-off, and approach, for the helicopter noise certification testing. However, the above-mentioned method can not be applied to the conditions of high-speed forward flight and descending flight at present because two types of impulsive noise occur in these conditions. One of them is high-speed impulsive (HSI) noise and the other is blade-vortex interaction (BVI) noise. The calculation methods of impulsive noise are described in the following sections, 2.3.2 and 2.3.3.

2.3.2 HSI noise

The prediction method of far field HSI noise is based on the combined method[14] of CFD technique with the Kirchhoff's equation. In this method, the Euler code mentioned above is used to obtain the pressure distribution around a rotor blade. The Kirchhoff's equation extended for a moving surface is then used to find the acoustic pressure at a far-field observer position. The Euler solutions on the Kirchhoff surface, in which all the acoustic sources are enclosed, are used as source pressure data. If the CFD solutions capture the nonlinear effect such as shock wave, the acoustic pressure including the effect of nonlinear sources can be obtained by this method. In this study, the Euler code, which has the good capability of capturing the shock wave by a higher-order upwind scheme, is used for the CFD calculation. The Kirchhoff surface used here is selected to correspond with the finite difference grid used in the CFD calculation. The size of the surface was determined by a preliminary size sensitivity study.

2.3.3 BVI noise

The prediction method[15] of BVI noise consists of the following four steps: 1) trim analysis using CAMRAD II based on a lifting-line theory, 2) interpolation of the blade motion and the wake geometry, 3) aerodynamic analysis using a finite difference solver for the three-dimensional unsteady Euler equations, and 4) noise analysis using an aeroacoustic code based on the Ffowcs Williams and Hawkings (FW-H) formulation. In the first step, the blade motion and the wake geometry are obtained as the result of the free-wake analysis of CAMRAD II. The calculation is done in every 15-deg. azimuthal position. However, it is too coarse to capture the instantaneous BVI phenomenon. Therefore, the azimuthal resolution is improved to 1 deg. in the second step. In the third step, the Euler solver mentioned above is applied. The effect of the wake is modeled by using the angle-of-attack approach in which the effect of the disturbance caused by the blade-vortex interaction is only felt through the surface boundary condition. The effective angle of attack obtained in the second step is used in this boundary condition. In the fourth step, the aeroacoustic code utilizes the FW-H formulation without the quadrupole term because strong shock waves are not generated in the flight condition considered here. The acoustic pressure at an observer position is calculated by using the pressure distributions on the blade surface obtained in the third step.

3. Design of low noise rotor

3.1 Design Concept

The dimension of the basic rotor of ATIC is shown in Table 1. The reduction of rotor rotational speed and the use of a 5-bladed rotor are the main concept for the design of a low noise rotor in this study. However, the reduction of rotor rotational speed widens the stall region in the retreating side of a rotor and induces vibration. Therefore, a blade named AT1, which effectively delays the occurrence of stall, is newly developed by improving the characteristics of airfoil and tip planform as mentioned in the following sections. Two airfoils, AK080A and AK100D (see Figure 4), are designed and applied to the blade. The thickness ratios of the airfoils are 8% and 10%, respectively. The tip planform, $J2_{mod}$, is also designed and applied to the blade. The wind tunnel test of the 1/3-scaled model of AT1 rotor will be performed at DNW in the beginning of 1998. In addition, ATIC regards HHC, active flap, and noise abatement flight operations as the candidates for the techniques of BVI noise reduction.

3.2 Airfoils

Two types of airfoils have been designed by taking account of not only aerodynamic but also aeroacoustic characteristics for the purpose of newly developing a low noise rotor.

From the aerodynamic point of view, the airfoils for rotor blades are required to have high lift performance on the retreating side, low drag performance on the advancing side, and high L/D performance in the other azimuthal region. The objective of the airfoil design in this study, therefore, is to increase the maximum lift coefficient (C_{lmax}) in low Mach number cases, the lift to drag ratio (L/D) in medium Mach number cases, and the drag divergence Mach number (M_{dd}) in high Mach number cases. In addition, the pitching moment coefficient at zero lift (C_{mo}) is monitored in order not to exceed the proper value in

the design process.

From the aeroacoustic point of view, the airfoils for rotor blades should be designed to suppress the suction peak at the leading-edge in low Mach number cases. The suppression increases C_{lmax} and reduces the rotational noise. Moreover, the airfoils for rotor blades should be designed to satisfy the Peaky type pressure distribution in high Mach number cases. Such a pressure distribution increases M_{dd} and reduces the HSI noise.

The new airfoil, AK080A (t/c=8%), illustrated in Figure 4(a) is designed in order to satisfy the above mentioned requirements in low and high Mach number cases. On the other hand, the new airfoil, AK100D (t/c=10%), illustrated in Figure 4(b) is designed in order to satisfy the requirements in low and medium Mach number cases.

The aerodynamic characteristics of the airfoils are measured by the wind tunnel tests[16] conducted in the NAL two-dimensional Transonic Windtunnel. Figure 5 shows the zero lift drag coefficient (C_{do}) of AK080A with freestream Mach number. It is indicated that M_{dd} of AK080A is about 0.87. Figure 6 shows the lift coefficient (C_l) of AK100D with angle of attack. It is indicated that C_{lmax} of AK100D is about 1.47 in the case of M=0.4. The obtained characteristics of AK080A and AK100D are plotted and compared with those of some existent airfoils for helicopters in Figure 7. It can be concluded from this figure that our design of AK080A and AK100D is completed successfully. In addition, it is also confirmed[16] that AK080A and AK100D show desirable performances both in L/D and C_{mo} compared with those of NACA23012 $_{mod}$ airfoil, which is applied to BK117.

3.3 Tip planform

At the first stage of the tip-planform design, two types of tip planform are selected and investigated experimentally. One of them is F1, which has the planform similar to that of BERP without roundness as illustrated in Figure 8. This planform is selected because the main requirement of our tip-planform design is to increase the stall angle in order to make it possible to reduce the rotor rotational speed. The other planform is NA1, which is developed by NAL in order to restrict the shock-wave generation on the advancing side of a helicopter rotor. Its planform is illustrated in Figure 8. The features[17], a large sweep-back and a delta-shape extension of the leading edge, effectively delays the generation of shock wave and the occurrence of delocalization. Therefore, the planform reduces the HSI noise.

The wind tunnel test for the fixed wing models of NA1 and F1 was conducted in 2m ϕ Low Speed Windtunnel of Japan Aircraft Co., Ltd. The measurements of force and moment are performed at the condition of Re = 5.1 x 10^5 and M = 0.1. The models of the wind tunnel test are untwisted and the airfoil sections are VR-XX series. The authors assume that the qualitative evaluation of the performance of tip planform is possible[18] by a fixed wing model test although the effects of rotor rotation, centrifugal force, and Coriolis force are not taken into account.

Figure 9 shows the C_L-α curves of NA1 and F1. The stall angle of F1 is about 14° and it is less than that of NA1. However, F1 gives smaller drop of C_L caused by stall compared with NA1. Moreover, stall angle of F1 increases up to 26° after the first stall. This phenomenon is due to the vortex generated by the notch. It is reported[19] that the notch of BERP tip generates the vortex at high angle of attack which prevents the flow separation in the tip region.

At the next stage of the tip-planform design, four types of planforms, F1, F2, F6, and F19, in Figure 10 are compared. The results are shown in Figure 11. The drop of C_L around α=14° obtained by F6 is the smallest of the four. It is assumed that the round notch and sweepback generate the vortices which prevent the flow separation at high angle of attack.

At the final stage of the tip-planform design, three types of planforms, $F6_{mod}$, J1, and J2, in Figure 12 are compared. Both J1 and J2 have "notched" trailing edge in order not to increase the chord length without losing the benefit of leading-edge notch. The results of C_L-α curve are shown in Figure 13. It is indicated that the modification of trailing edge does not strongly affect the stall characteristic. Figures 14 and 15 show C_L-C_D and C_M-α curves, respectively. The moment characteristic of J2 is good although that of J1 is not acceptable.

As a result of the above-mentioned experimental investigations, J2 is chosen as the candidate of the new tip planform. After a minor modification of the trailing-edge of J2, a newly designed tip planform, $J2_{mod}$, is obtained. The airfoils, AK080A and AK100D, and the tip planform, $J2_{mod}$, are integrated into a new blade, AT1, shown in Figure 16. The aerodynamic characteristics of the tip region of AT1 was measured in 1m x 1m Transonic Windtunnel of Kawasaki Heavy Industries, Ltd. Figures 17(a), (b), and (c) show C_L-α, C_L-C_D, and C_M-α curves of AT1 and a rectangular blade at M=0.4, respectively. The rectangular blade has the AK080A airfoil section. The model of AT1 shows better characteristics than that of the rectangular blade in the three figures. The increase of the stall angle by AT1 derives the conclusion that the aim of the tip-planform design by ATIC is accomplished.

3.4 Description of model rotor

The aerodynamic and aeroacoustic characteristics of the 1/3-scale model of the AT1 rotor will be studied experimentally in DNW in the beginning of 1998. The model rotor is 4 m in diameter and the number of blades is five. Figure 18 shows the model rotor installed in NAL Low Speed Windtunnel. The blade

planform is shown in Figure 19(c). The effect of number of blades can be evaluated by replacing the 5-bladed rotor with a 4-bladed one. Another two types of blades shown in Figures 19(a) and (b) will be also tested. One of them is the basic blade with a rectangular tip planform and the other is the blade with a planform similar to the BERP tip. The distributions of their thickness, chord length and twist are shown in Figure 20. The normal rotational speed of the testing will be 1002.7 rpm and the range of the rotational speed will cover from 840 rpm to 1050 rpm. Moreover, this rotor system has HHC actuators which cover 0-105 Hz for frequency range and ± 2 deg. for amplitude range.

4. Evaluation of AT1 rotor

4.1 Prediction of rotor performance

The prediction method of rotor performance explained in Section 2.1 is used here. The performances of the model rotors with the rectangular and AT1 tip planforms are predicted using CAMRAD II. The blades are assumed to be rigid. The effect of the tip shape on the occurrence of stall is introduced by modifying the C_l-α curve used in CAMRAD II. Such a modification is not applied to the C_m-α and C_d-α curves. The tip vortex shed from $J2_{mod}$ is assumed to be formed at r/R=0.99 because $J2_{mod}$ is highly tapered at the tip region. The calculations are performed in hover and forward flight. The predicted performances in hover and forward flight conditions are shown in Figures 21(a) and (b) respectively. The power of AT1 is reduced by 15-20% compared with that of the basic blade both in hover and forward flight conditions. The main reason is the improvement of L/D by AT1.

4.2 Prediction of rotor noise

4.2.1 Rotational noise in forward flight

The prediction method of the rotational noise explained in Section 2.3.1 is used here. The rotational noises of the following four rotors are calculated and compared: 1) 5-bladed rotor with rectangular tip rotated by normal rotational speed, 2) 4-bladed rotor with rectangular tip rotated by normal rotational speed, 3) 5-bladed rotor with rectangular tip rotated by 10%-reduced rotational speed, 4) 5-bladed rotor with AT1 tip rotated by normal rotational speed. The operational condition is as follows: V = 120kt and C_T = 0.0064. Predicted waveforms are shown in Figure 22. The observer position is illustrated in the figure. The figure indicates that the 4-bladed rotor is much noisier than the 5-bladed rotor. However, it should be noticed that the blade loading of the 4-bladed rotor is larger than that of the 5-bladed rotor in this calculation. It is also indicated that the most effective factor for noise reduction is rotor rotational speed as expected at the first stage of our study. Although the rotational noise is not reduced by the AT1 tip shape alone as shown in Figure 22(d), it is assumed that the AT1 rotor reduces the rotational noise because it is used on the condition of reduced rotor rotational speed.

4.2.2 HSI noise

The prediction method of the HSI noise explained in Section 2.3.2 is used here. All the calculations in this section are performed on the non-lifting hover condition of M_{tip} = 0.9. The calculated blades are untwisted. The aspect ratio of each blade is 13.71. The Kirchhoff surface is located at 1.099R in the spanwise direction and 1.5c away from the quarter-chord line of the blade. The distance between the hub center of the rotor and the observer position is 3.0R.

Figure 23(a) compares the waveforms of the HSI noise generated by the following two rotors. One of them has a rectangular tip planform with AK080A airfoil section and the other has a rectangular tip planform with NACA0008 airfoil section. There is less difference between the waveforms. Therefore, it is indicated that the effect of the airfoils on the HSI noise is small. Figure 23(b) compares the waveforms generated by the following two rotors. One of them has a $J2_{mod}$ tip planform with NACA0012 airfoil section and the other has a rectangular tip planform with NACA0012 airfoil section. The absolute value of the negative peak pressure obtained by the former one is about half of that obtained by the latter one. Therefore, it is indicated that the effect of the planforms on the HSI noise is large. Figure 23(c) compares the waveforms generated by the following two rotors. One of them has the AT1 blade and the other has the basic blade. The former one reduces the negative peak pressure by about half compared with the latter one. It is indicated that the AT1 rotor effectively reduces the HSI noise. Figure 25 shows the calculated Mach contours around the two blades. It is clearly observed that the occurrence of delocalization is prevented by the AT1 blade.

In addition, it should be noticed that the HSI noise intensity strongly depends on the aspect ratio of the rotor blade because it is firmly related to the area of the supersonic region on the blade surface in the tip region.

4.2.3 BVI noise

The prediction method of the BVI noise explained in Section 2.3.3 is used here. The calculations are performed for the four rotors mentioned in Section 4.2.1. The core radius of the tip vortex is assumed to be 0.2c in each case.

Figure 25 shows the calculated waveforms of BVI noise on the condition of V=50kt, C_T=0.0064, and α_{tpp}=2° (AFT). The basic 5-bladed rotor is noisier than the 4-bladed rotor since the 5-bladed rotor causes more BVIs compared with the 4-bladed rotor as

shown in Figure 26. This figure shows the top views of the calculated BVI locations for the two rotors. The open and solid circles represents the interaction above and below the rotor disk, respectively. The miss-distance is indicated by the size of the circle. The larger the circle is, the shorter the miss-distance between blade and vortex is. In Figure 25, it is indicated that both the reduction of rotor rotational speed and the usage of AT1 are effective for the reduction of the BVI noise. Therefore, it is assumed that the AT1 rotor, which is operated by the reduced rotor rotational speed and uses the AT1 blades, reduces the BVI noise with no performance penalty.

In addition, the tip vortex structure is analyzed by the Navier-Stokes solver explained in Section 2.2. Figure 27 shows the vorticity contours behind the AT1 blade and a rectangular blade with the NACA0012 airfoil section. The plane on which the contour is shown is located 1-chord behind the trailing-edge of the rectangular blade in each case. Each blade has no twist and the aspect ratio is 6.0. The blade tip Mach number is 0.4. The collective pitch angle, θ c, is set to 10° for the AT1 blade and 11.234° for the rectangular blade in order to equalize the thrust. It is clearly observed that the tip vortex of rectangular tip is more concentrated than that of the AT1 tip.

5. Conclusions

Two airfoils, AK080A and AK100D, and a tip planform, $J2_{mod}$, are designed for the reduction of the helicopter external noise. They are integrated into a blade, AT1. The aerodynamic and aeroacoustic analyses of the AT1 rotor are performed using the several theoretical methods developed by the authors. The following conclusions are drawn.

- The results of some wind tunnel tests confirm that the performance of the airfoils and the tip planform satisfy the aerodynamic requirement by ATIC.
- The AT1 rotor reduces the power required by 15-20% compared with the basic rectangular blade.
- It is assumed that the AT1 rotor reduces the rotational noise because it is used on the condition of reduced rotor rotational speed.
- The AT1 blade weakens the shock wave on the blade and reduces the HSI noise at Mtip = 0.9.
- The AT1 blade reduces the intensity of the BVI noise in the condition of V=50kt, C_T=0.0064, and $\alpha_{tpp}=2^{\circ}$ (AFT).

All the results calculated here will be compared with the experimental data that will be obtained by the wind tunnel test in DNW in the beginning of 1998. However, the trade-off study between noise and performance is not completed at the present stage. After the first phase of the model rotor test at the DNW, the redesign of AT1 will be conducted considering the distributions of twist and airfoil along span-wise direction. The rotational speed of the rotor will be also reconsidered.

References

(1) International Civil Aviation Organization, First Meeting of the Committee on Aviation Environmental Protection (CAEP/1), Annex 16, Vol.I-2nd Edition, Amendment 3, Applicable 17 November 1988.

(2) James,H. and Philippe,J.J., A Quiet Helicopter, A Research Programme Today, A Reality Tomorrow, 20th European Rotorcraft Forum, No.9, 1994.

(3) Low Noise Design of the EC135Helicopter, 52nd Annual Forum of the American Helicopter Society, Vol.2, June 1996, pp.32-44.

(4) O'Connell,J., JanakiRam,R., and Hardesty,M., Noise Certification of the MD900 Explorer Helicopter, 52nd Annual Forum of the American Helicopter Society, June 1996.

(5) Kobiki,N., Murashige,A., Tsuchihashi,A., and Yamakawa,E., Elementary Study for the effects of Higher Harmonic Control on Blade Vortex Interaction, 23rd European Rotorcraft Forum, No.29, 1997.

(6) Murashige,A., Tsuchihashi,A., Tsujiuchi,T., and Yamakawa,E., Blade-Tip Vortex measurement by PIV, 23rd European Rotorcraft Forum, No.36, 1997.

(7) QTR-1,0.000.001.02, BK117 Qualification Test Report -Flight Test, 1982.

(8) Aoyama, T., Kawachi, K., and Saito, S., Unsteady Calculation for Flowfield of Helicopter Rotor with Various Tip Shapes, 18th European Rotorcraft Forum, No.B03, 1992.

(9) Aoyama,T., Saito,S., and Kawachi,K., Navier-Stokes Analysis of Blade Tip Shape in Hover, 16th European Rotorcraft Forum, No.1.4.1, 1990.

(10) Moriya,T., *Introduction of Aerodynamics*, Baifukan, 1972 (in Japanese).

(11) Nakamura,Y. and Azuma,A., Rotational Noise of Helicopter Rotors, Vertica, vol.3, no.3/4, 1979, pp.293-316.

(12) Brooks,T.F., Pope,D.S., and Marcolini,M.A., Airfoil Self-Noise and Prediction, NASA RP-1218, 1982.

(13) Hayama,K., Inagaki,K., Kondo,N., Yamakawa, E., and Masai,K., External Noise Measurement Test of the BK117 Helicopter, 33rd Aircraft Symposium, No.1C7, 1995 (in Japanese).

(14) Aoyama,T., Aoki,M., Kondo,N., Saito,S., and Kawachi,K., Effect of Blade-Tip Shape on High-Speed Rotor Noise, AIAA Paper 96-2380, 1996.

(15) Aoyama,T., Kondo,N., Aoki,M., Nakamura,H., and Saito,S., Calculation of Rotor Blade-Vortex Interaction Noise using Parallel Super Computer, 22nd European Rotorcraft Forum, No.8, 1996.

(16) Aoki,M., Kobiki,N., Yamakawa,E., Saito,S., Shigemi, M., Sato,M., and Kanda,H., Study on High-Performance/Low-Noise Airfoil of Helicopter Blade -

Two-Dimensional Transonic Wind Tunnel Tests, NAL-TM, to be published in 1997 (in Japanese).
(17) Aoyama,T., Kawachi,K., and Saito,S., Effect of Blade-Tip Planform on Shock Wave of Advancing Helicopter Blade, Journal of Aircraft, Vol.32, No.5, 1995, pp.955-961.
(18) Tsung,F., and Sankar,L.N., Numerical Simulation of Flow Separation for Rotors and Fixed Wings, AIAA Paper 92-0635, 1992.
(19) Perry, F.J., Aerodynamics of the Helicopter World Speed Record, 43rd Annual Forum of the American Helicopter Society, May 1987.

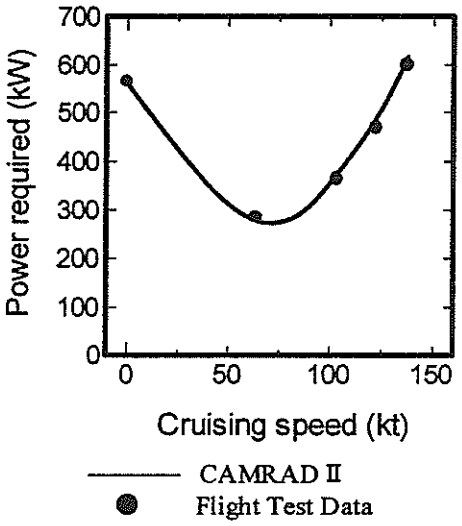

Figure 1 Performance of BK117.

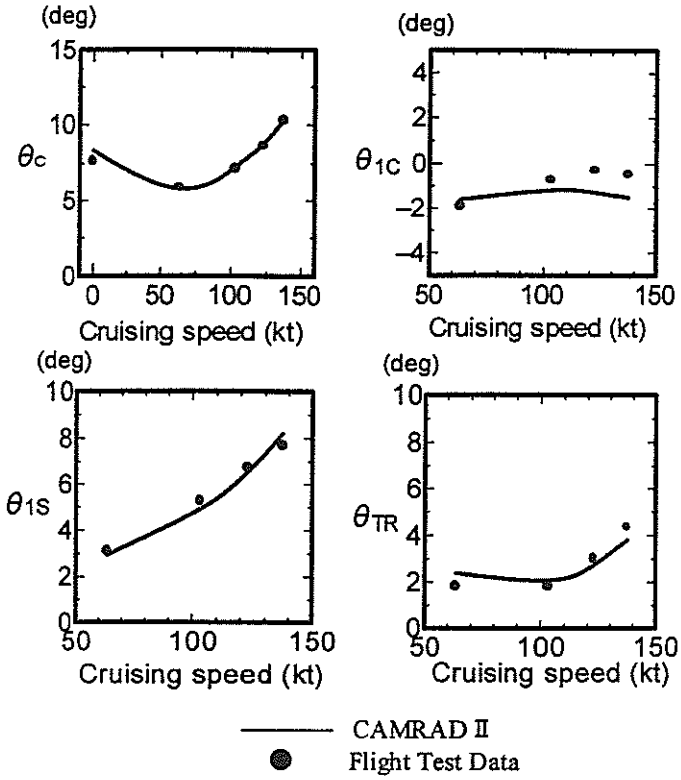

Figure 2 Control inputs of BK117.

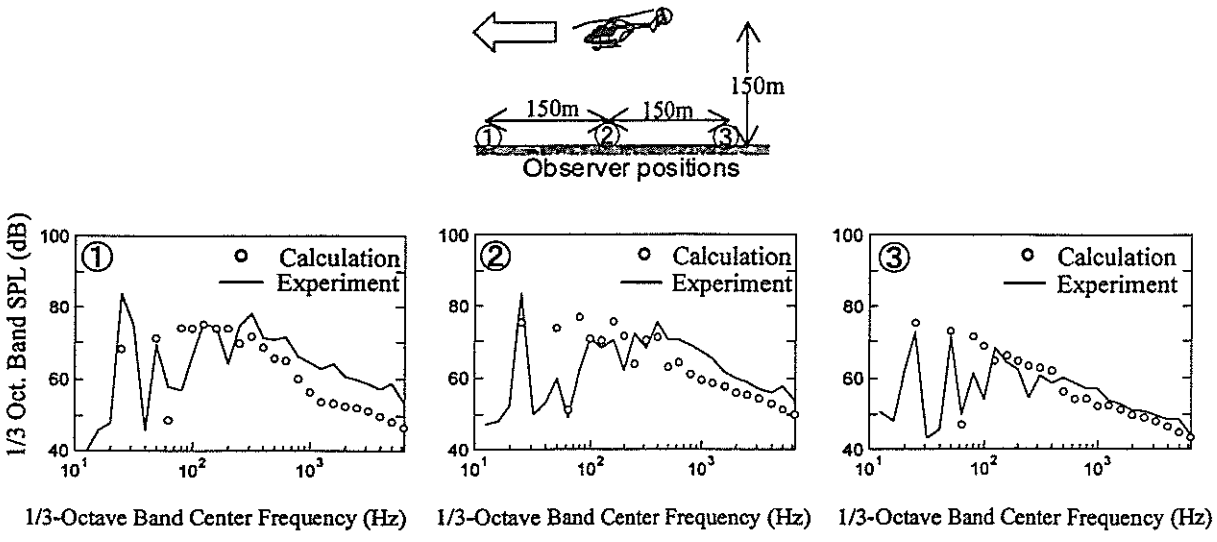

Figure 3. Noise spectrums of BK117 in forward flight (V=50kt).

Table 1 Dimension of basic rotor.

Rotor radius	6.0 m
Number of blade	5
Chord length (inboard)	0.382 m
Tip speed @ 100%RPM	210 m/s
Blade twist	-8 deg
Airfoil	$NACA23012_{mod}$
Tip planform	Rectangular

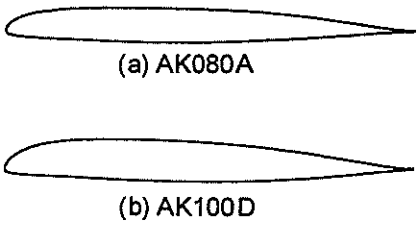

Figure 4 Geometries of new airfoils.

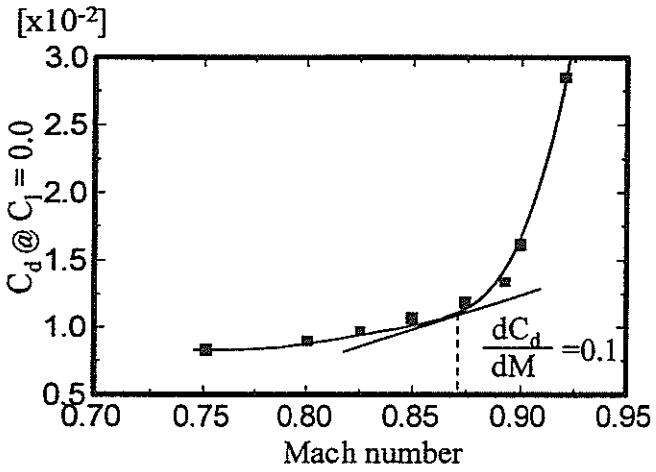

Figure 5 Drag coefficient of AK080A at zero lift with freestreem Mach number.

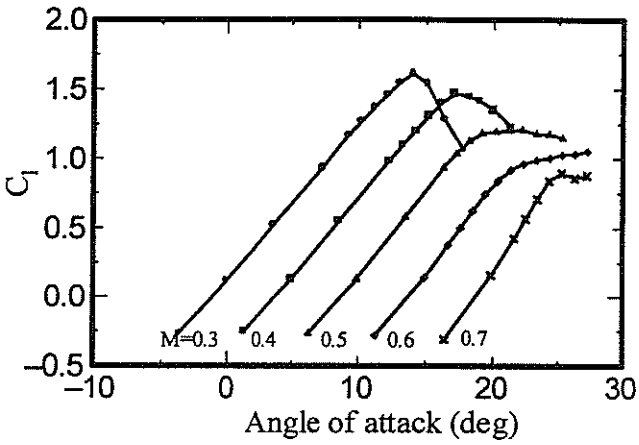

Figure 6 C_l-α curves of AK100D.

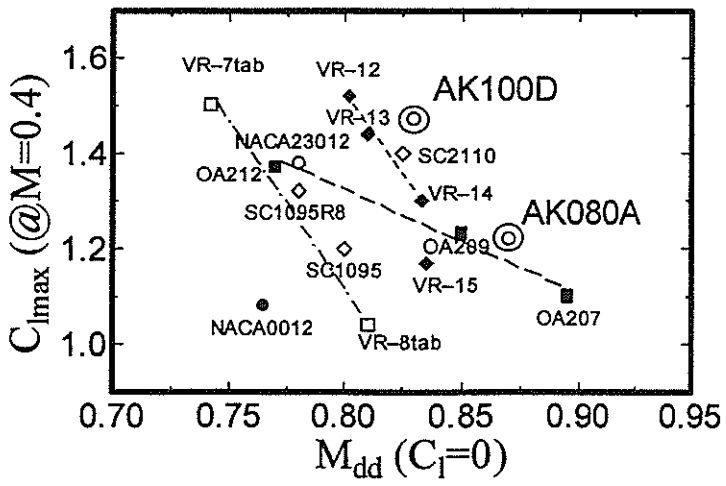

Figure 7 Performance of AK080A and AK100D compared with existent airfoils for helicopters.

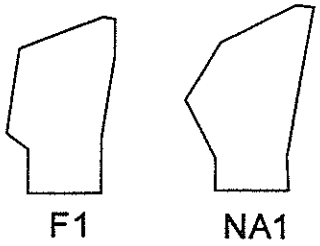

Figure 8 F1 and NA1 tip planforms.

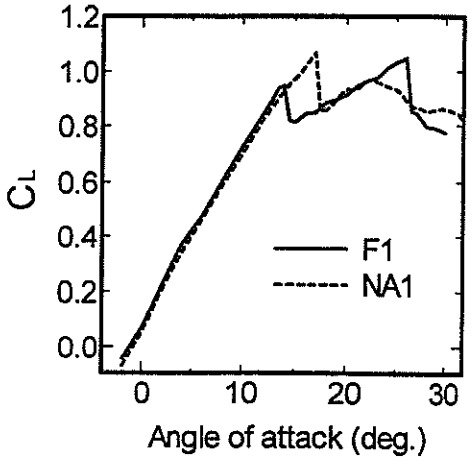

Figure 9 C_L-α curves of F1 and NA1 tip (M=0.1).

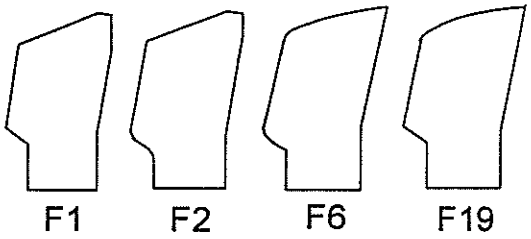

Figure 10 Various tip planforms.

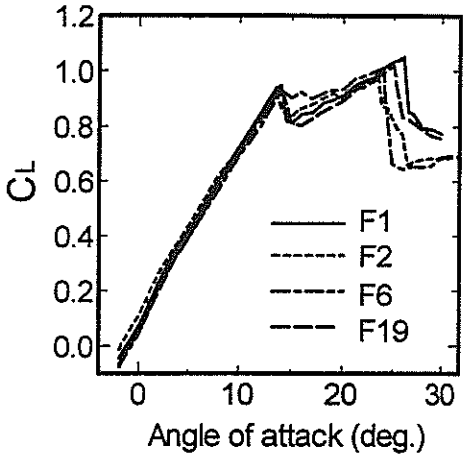

Figure 11 C_L-α curves of various tip planforms (M=0.1).

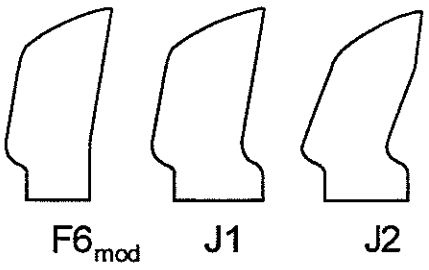

Figure 12 Selected tip planforms.

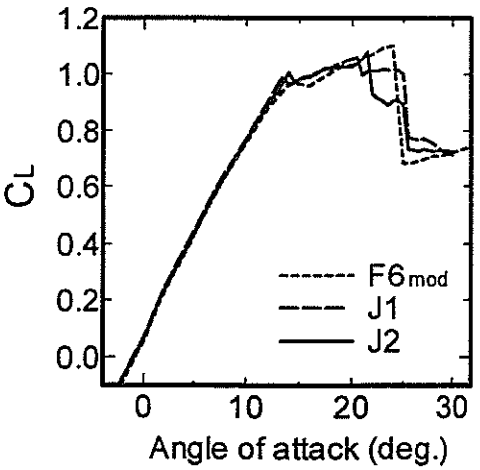

Figure 13 C_L-α curves of selected tip planforms (M=0.1).

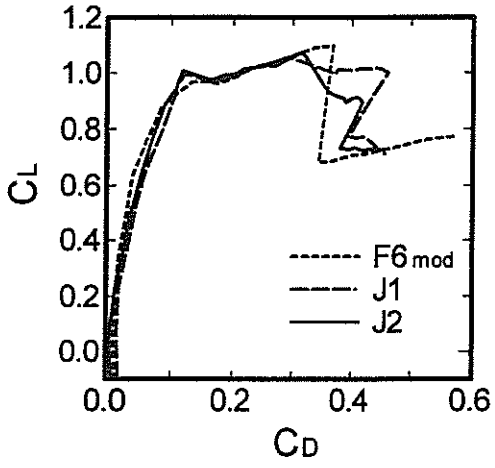

Figure 14 C_L-C_D curves of selected tip planforms (M=0.1).

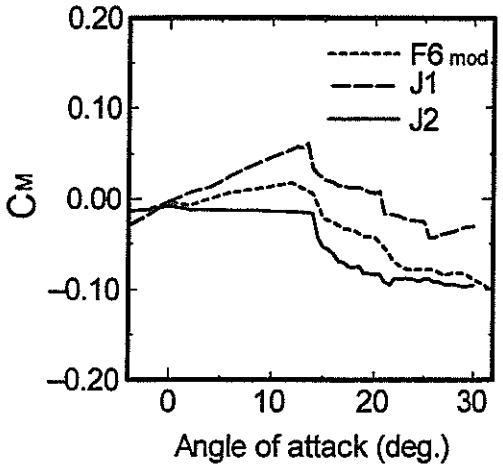

Figure 15 C_M-α curves of selected tip planforms (M=0.1).

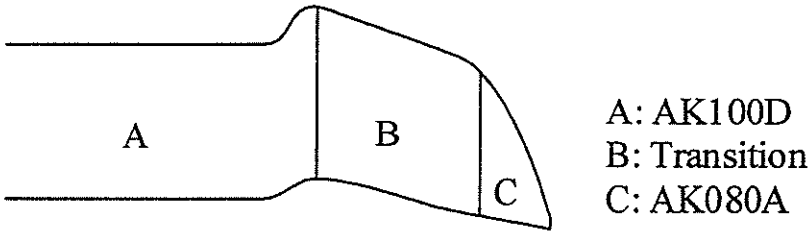

Figure 16 Planform of AT1 blade.

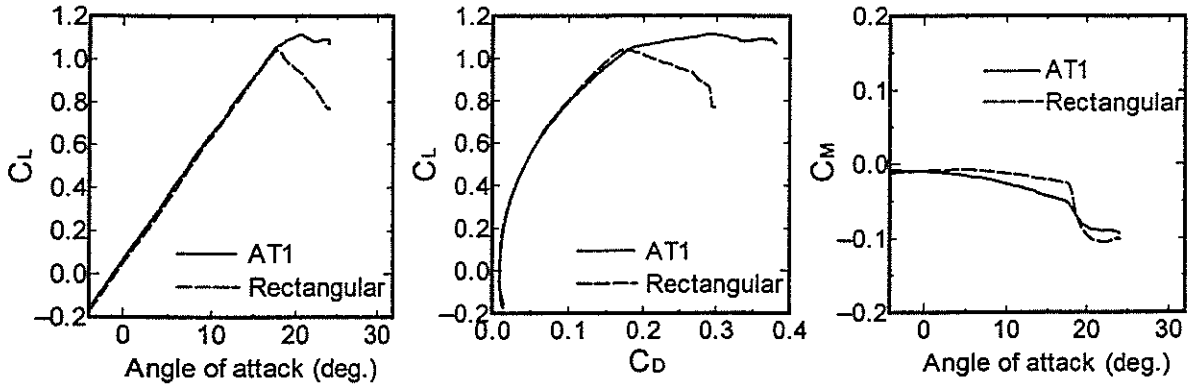

(a) C_L-α curves (b) C_L-C_D curves (c) C_M-α curves

Figure 17 Measured aerodynamic performance of AT1 and rectangular tips (M=0.4).

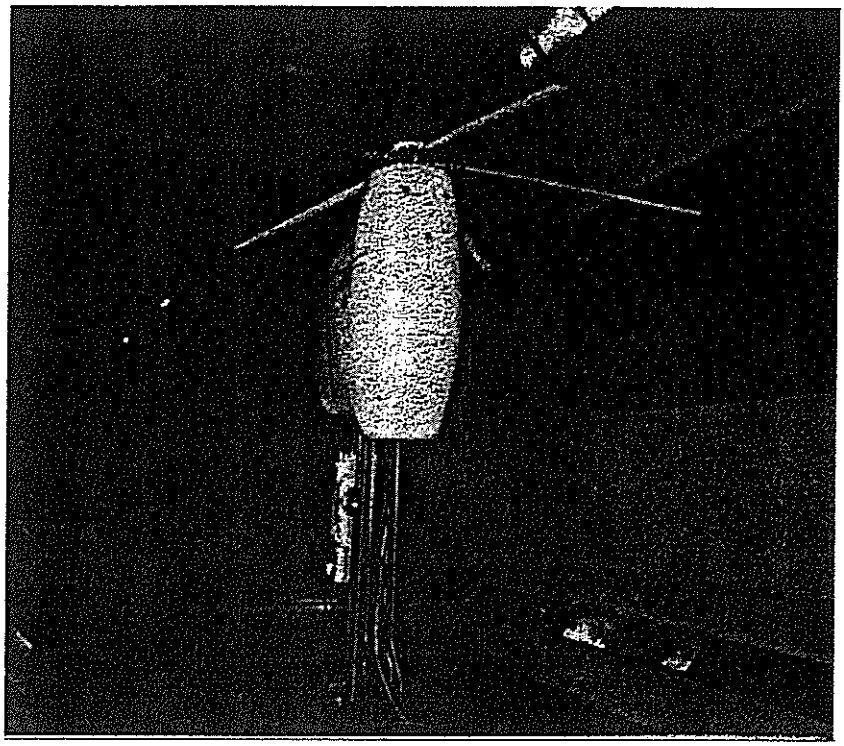

Figure 18 ATIC model rotor system in NAL Low Speed Windtunnel.

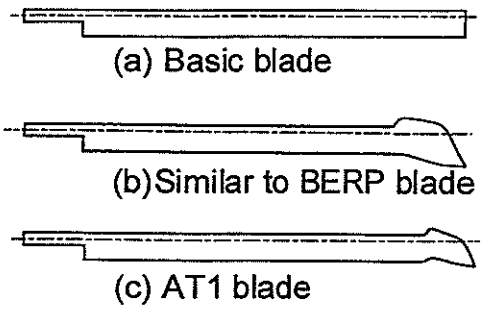

Figurer 19 Planforms of model rotor blades.

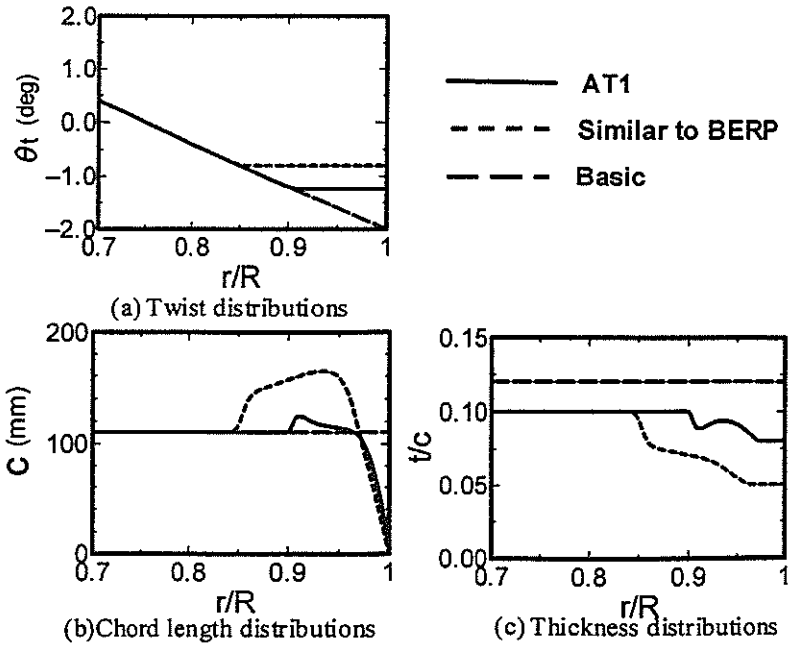

(a) Twist distributions

(b)Chord length distributions

(c) Thickness distributions

Figure 20 Geometries of model rotor blades.

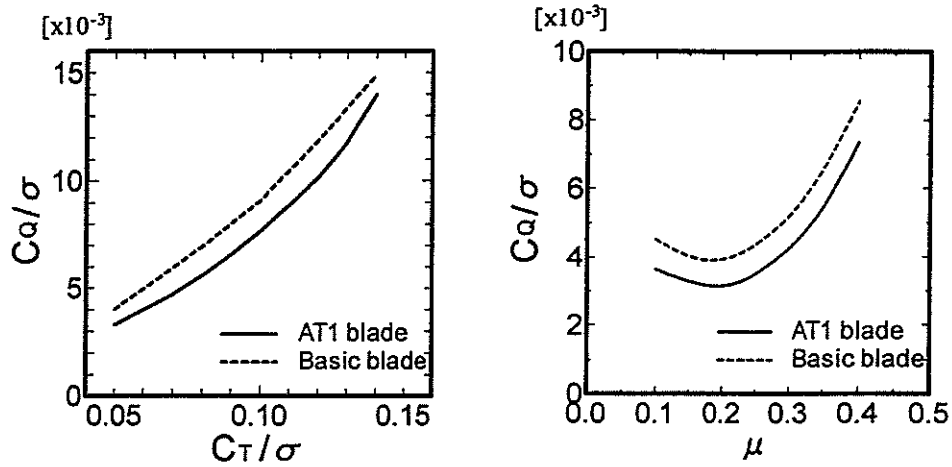

(a) Hover (b) Forward flight

Figure 21 Calculated performances of AT1 and rectangular blades (@100%RPM).

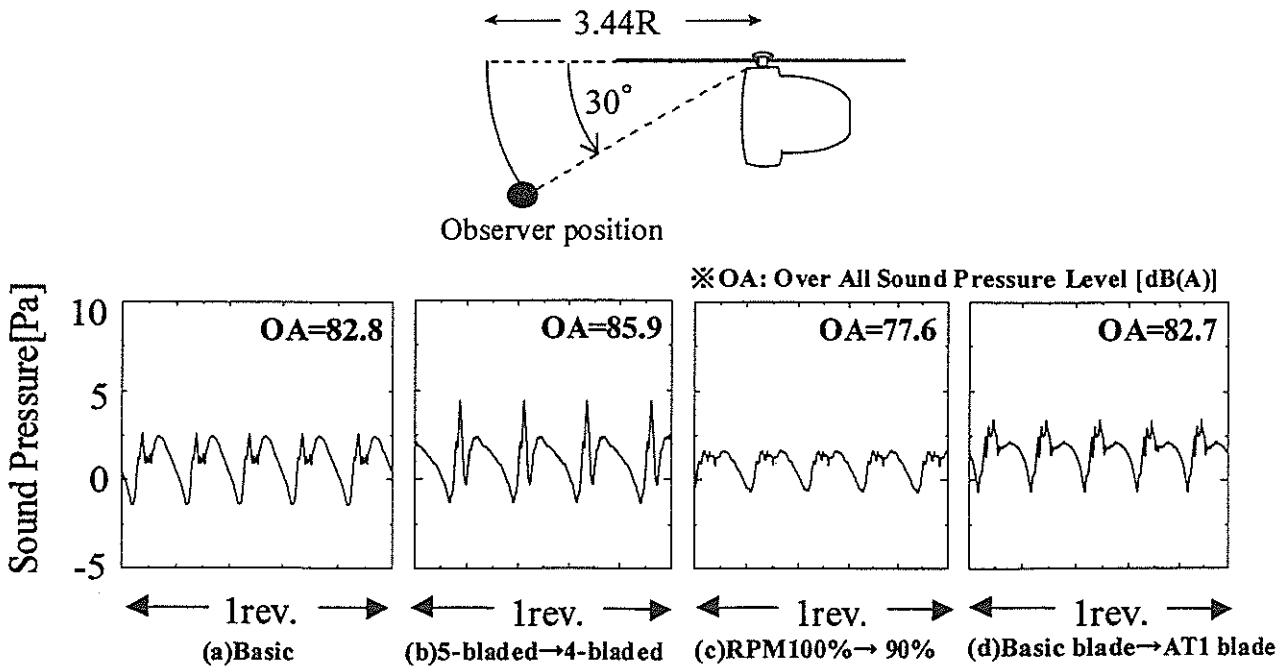

Figure 22 Calculated acoustic waveforms of model rotors (V=120kt, C_T=0.0064).

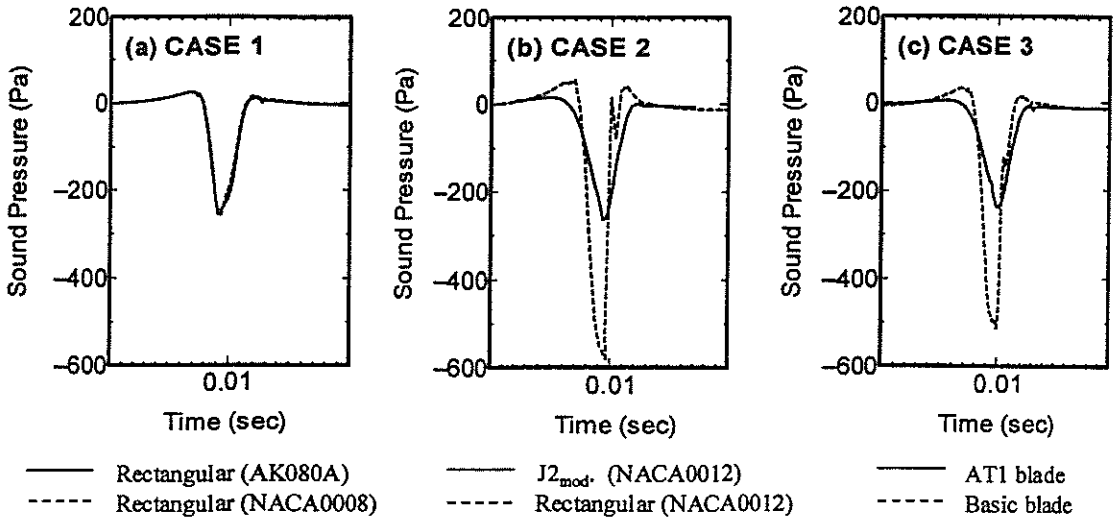

Figure 23 Calculated acoustic waveforms of HSI noise (M_{tip}=0.9, observer position 3.0R).

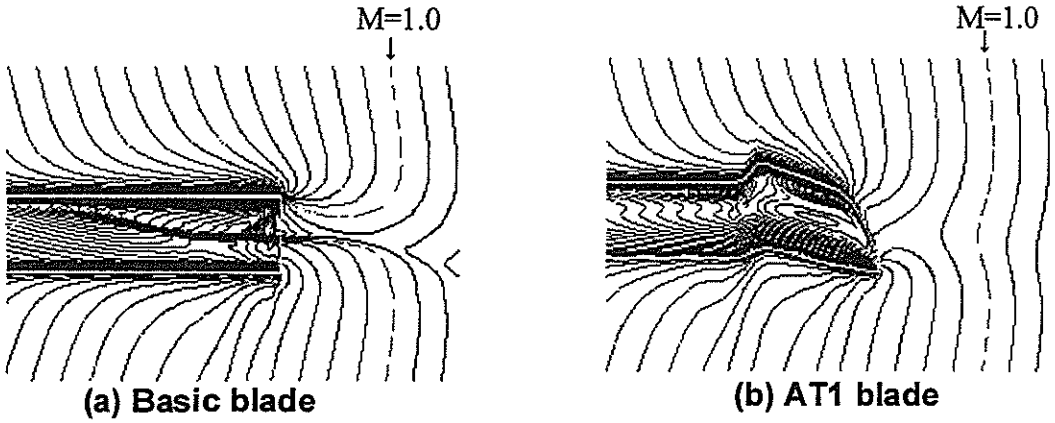

Figure 24 Comparison of calculated Mach contours for rectangular and AT1 blades.

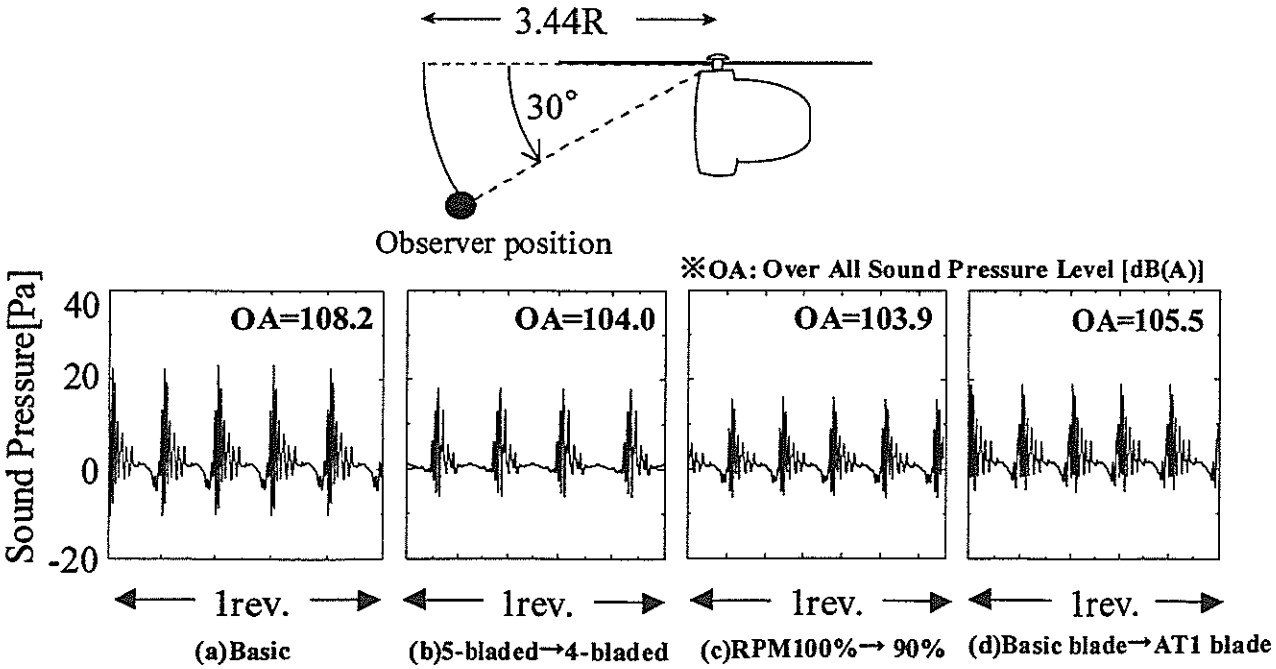

Figure 25 Calculated acoustic waveforms of BVI noise (V=50kt.,C_T=0.0064 , α_{tpp}=2deg AFT).

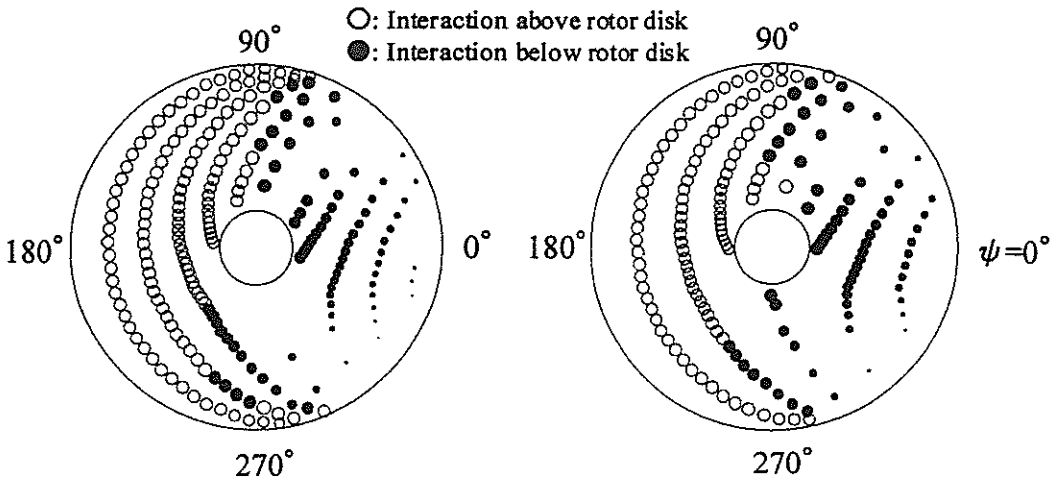

(a) 5-bladed rotor (b) 4-bladed rotor

Figure 26 Top views of calculated BVI locations of 5-bladed and 4-bladed rotors.

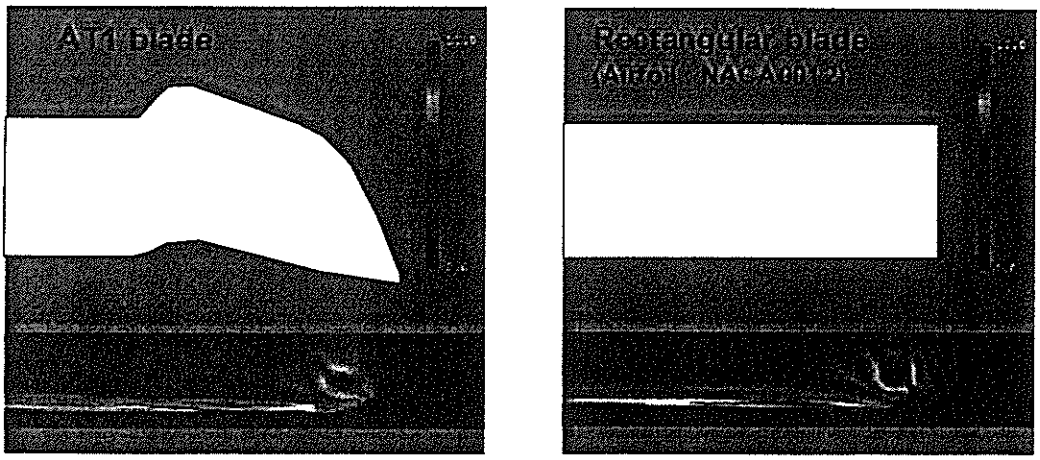

Figure 27 Vorticity contours at the plane located 1-chord behind trailing-edge.